

# Analyses of Missing Organs in Abdominal Multi-Organ Segmentation

Miyuki Suzuki<sup>1</sup>, Marius George Linguraru<sup>2,3</sup>,  
Ronald M. Summers<sup>2</sup>, and Kazunori Okada<sup>1</sup>

<sup>1</sup> Department of Computer Science  
San Francisco State University  
{miyukis,kazokada}@sfsu.edu

<sup>2</sup> Radiology and Imaging Sciences  
National Institutes of Health Clinical Center  
{lingurarum,rsummers}@mail.nih.gov

<sup>3</sup> Sheikh Zayed Institute for Pediatric Surgical Innovation  
Children's National Medical Center

**Abstract.** Current methods for abdominal multi-organ segmentation (MOS) in CT can fail to handle clinical patient population with missing organs due to surgical removal. In order to enable the state-of-the-art atlas-guided MOS for these clinical cases, we propose 1) statistical organ location models of 10 abdominal organs, 2) organ shift models that capture organ shifts due to specific surgical procedures, and 3) data-driven algorithms to detect missing organs by using a normality test of organ centers and a texture difference in intensity entropy. The proposed methods are validated with 34 contrast-enhanced abdominal CT scans, resulting in 80% detection rate at 15% false positive rate for missing organ detection. Additionally, the method allows the detection/segmentation of abdominal organs from difficult diseased cases with missing organs.

**Keywords:** multi-organ segmentation, contrast-enhanced CT.

## 1 Introduction

Segmentation of abdominal organs is a crucial building block for computer-aided diagnosis (CAD) of various diseases in CT and also a major technical challenge due to similar intensity of neighboring organs and high inter subject variability of organ's geometry [4]. Addressing this challenge, multi-organ segmentation (MOS) approach has recently become popular toward improving overall segmentation accuracy and enabling comprehensive analysis of multi-focal abdominal diseases [10, 15, 13, 9, 12, 14, 6–8].

In this paper, we investigate how such MOS can be extended to a patient population with missing organs. Without considering this population, MOS cannot be applied to a number of important clinical applications such as follow-up studies of surgical treatment and cancer recurrence in abdomen. Despite this clinical importance, however, the literature discussing how MOS performs with data from such population is lacking. Current MOS solutions are also not designed to handle irregular anatomy cases. A common process in various MOS methods

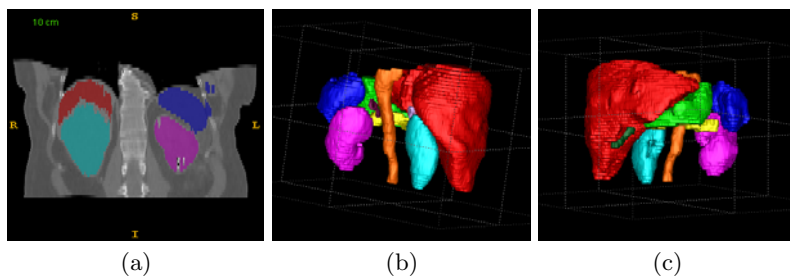


**Fig. 1.** Illustrative examples of a) segmentation failures and b,c) ten modeled organs. Red: liver, blue: spleen, cyan: r-kidney, magenta: l-kidney, yellow: pancreas, orange: aorta, dark green: gall bladder, purple: l-adrenal, lavender: r-adrenal, green: stomach.

is to fit an atlas of normal organ anatomy to an image to be analyzed. When analyzing a case with missing organs, regardless of atlas formats (i.e., static [15], probabilistic [10, 13, 9, 6, 7], or geometric [13, 12, 14, 6, 8]), MOS can fail to segment other intact organs because of 1) post-surgical organ shifts and 2) mis-match of the atlas' part corresponding to the missing organs to nearby non-targets. As a result, these MOS methods applied to missing organ cases can underperform organ-specific segmentation schemes. Fig.1(a) illustrates such a case with a missing right kidney (cyan) where the liver (red) shifted downward into the cavity caused by the removed kidney and a part of the liver was identified as kidney. The main contribution of this paper is two-fold. First, surgical procedure-specific organ shift models are proposed and built using nine clinical cases of nephrectomy (kidney removal) and splenectomy (spleen removal). 3D centers of ten abdominal organs are first estimated by a geometric Gaussian mixture model (GMM) then statistically modeled with respect to normal organ locations. Second, two new features for data-driven missing organ detection are proposed. As a base MOS, the atlas-guided MAP algorithm proposed in [13] is used, which fits a GMM with a probabilistic atlas constructed from ten normal organ cases. One feature characterizes the probability of each segmented organ being normal by using statistical organ location models, while the other feature examines the intensity entropy under an atlas mask and compares it against normal anatomical organs. The automatic missing organ detection allows us to handle clinical scan data more robustly even when previous medical history information is missing or corrupted in patient record or DICOM tag [2]. The proposed method is related to a multi-organ identification framework [3, 5, 14] such as the spine-based statistical location model (SLM) proposed by Yao and Summers [14]. This paper focuses on applying the SLM approach to the missing organ cases as a pre-step of MOS.

## 2 Method

### 2.1 Atlas-guided MAP Multi-Organ Segmentation

We follow Shimizu et al. [13] as our base atlas-guided MOS method. The MAP estimation of organ label  $l \in \{1, \dots, L\}$  over 4D spatiointensity feature vector  $\mathbf{v} =$

$(x, y, z, I(x, y, z))$  is employed:  $\hat{l} = \operatorname{argmax}_l p(\mathbf{v}|l)p(l)$ . A standard probabilistic atlas [10, 7] is built by registering  $K$  training cases of normal anatomy to a fixed reference volume  $I_R$  then computing a probability map for each of  $L$  modeled organs by counting segmented organs. The prior  $p(l)$  is modeled by this atlas. For each organ  $l$ , a normal spatiointensity model  $(\mathbf{u}_{\mathbf{v}l}, \Sigma_{\mathbf{v}l})$  is also computed where  $\mathbf{u}_{\mathbf{v}l}$  and  $\Sigma_{\mathbf{v}l}$  are the mean and covariance of feature vectors of the organ  $l$  from the  $K$  training cases. The likelihood  $p(\mathbf{v}|l)$  is modeled by an extended GMM  $p(\mathbf{v}) = \sum_{l=1}^L \left( \frac{1}{N} \sum_{n=1}^N \alpha_l(n) \right) N(\mathbf{v}; \mathbf{u}_l, \Sigma_l)$  where  $N$  denotes the number of voxels and the mixing weights  $\alpha_l(n)$  are defined over each voxel  $n$ . To segment  $L$  organs in a test case  $I_{te}$ ,  $I_{te}$  is first registered to  $I_R$  using affine transformation followed by B-spline non-rigid registration [11]. Then the GMM is initialized by the normal spatiointensity model and fit to  $I_{te}$  using the EM-algorithm [1].

## 2.2 Organ Location and Shift Models

Geometry of abdominal organs varies due to a) inter-subject variation, b) post-surgical organ shifts, c) postures and d) pathology. Focusing on modeling the first two factors, we prepare a set  $\{I_m^{na} | m = 1, \dots, M_{na}\}$  with  $L$  normal anatomy and a set  $\{I_{m'}^{mo} | m' = 1, \dots, M_{mo}\}$  with one or two organs missing. After registering all cases to  $I_R$ , each organ's location is modeled by the point distribution density of organ centers  $\mathbf{x}_{lm}$ , each of which is given by either the segmented organ's median coordinate or expert's manual estimation. Organ location models (OLMs) for normal anatomy (NA) and for missing organs (MO) are built as a set of normal densities over  $M_{na}$  NA and  $M_{mo}$  MO cases, respectively

$$NA = \{NA_l\} = \{N(\mathbf{x}; \mu_l, \Sigma_l) | l = 1, \dots, L\} \quad (1)$$

$$MO = \{MO_l\} = \{N(\mathbf{x}; \mu'_l, \Sigma'_l) | l = 1, \dots, L\} \quad (2)$$

where  $\mu_l = 1/M_{na} \sum_m \mathbf{x}_{lm}$ ,  $\mu'_l = 1/(M_{mo} - \#MO_l) \sum_{m'} \mathbf{x}_{lm'}$ ,  $\#MO_l$  denotes the number of missing cases for organ  $l$ , and  $\Sigma_l$  and  $\Sigma'_l$  are covariance matrices corresponding to  $\mu_l$  and  $\mu'_l$ , respectively.

While both NA and MO model the inter-subject variation of organ locations, MO is also influenced by the post-surgical organ shifts. Organ shift model (OSM) is then designed by a set of normal point-difference distributions  $\{\mathbf{y}_{lm} = \mathbf{x}_{lm} - \mu_l\}_l$  in a local frame centered at  $\mu_l$  for each organ  $l$

$$OS = \{OS_l\} = \{N(\mathbf{y}_l; \mu'_l - \mu_l, \Sigma'_l) | l = 1, \dots, L\} \quad (3)$$

Surgical procedure-specific organ shift models  $\{OS_t | t = 1, \dots, T\}$  where  $T$  is the number of organ-specific missing cases are modeled by computing an OSM in Eq.(3) with a subset of the MO cases specific to a surgical procedure such as nephrectomy and splenectomy. OSM can take two different variations according to their purposes; anatomical and detectional OSM. Anatomical OSM is created by manually estimated organ centers which visualize true post-surgical organ shifts. Whereas detectional OSM applies centers estimated by EM algorithm which detects the failure of EM algorithm for missing organs and this used as a part of our missing organ detection method.

### 2.3 Missing Organ Detection

When fitting the GMM  $p(\mathbf{v})$  described in Sec 2.1 to a missing organ case  $I^{mo}$ , a normal model corresponding to a missing organ will be fitted to arbitrary non-target organ(s) located nearby. Data-driven detection of such missing organs can therefore be used to mitigate this EM estimation error. Each organ in the atlas is first linearly translated to the center estimated by EM algorithm for each NA and MO cases resulting in organ-specific binary atlas masks  $B_l(\mathbf{x})$ .

The first indicator feature  $F_l$  of missing organ  $l$  is the probability of estimated organ centers by EM being abnormal with respect to estimated organ centers of NA,

$$F_l = 1 - p(x|\theta_l) = 1 - N(x; \mu_l, \Sigma_l) \quad (4)$$

where  $\theta_l = (\mu_l, \Sigma_l)$ .

The second indicator feature  $G_l$  examines the difference in texture pattern under the atlas mask  $B_l(\mathbf{x})$  comparing entropies of MO to NA and scales it to the same range as  $F_l$ ,

$$G_l = 1 - e^{-|E_l - E_l^{NA}|} \quad (5)$$

where  $E_l$  and  $E_l^{NA}$  denote intensity entropy computed with the MO case  $I^{mo}$  and with the NA cases  $\{I_m^{na}\}$  masked by  $B_l(\mathbf{x})$ , respectively.

## 3 Experiments

### 3.1 Data

Nine MO ( $M_{mo}=9$ ) and twenty five NA ( $M_{na}=25$ ) cases, totaling 34 contrast-enhanced diseased abdominal CT scans, are used in this study. Each scan consists of  $512 \times 512 \times 50$  voxel slices with 5mm thickness stored in Mayo analyze format. CT scanners from various manufacturers are used to acquire this dataset with the ISOVUE 300 contrast agent. The MO dataset contains three different types of surgical organ removal: i) 5 splenectomy cases (spleen removed), ii) 3 nephrectomy cases (right kidney removed), and iii) 1 splenectomy and nephrectomy case (spleen and left kidney removed). Ten abdominal organs ( $L = 10$ ) are considered in this study: aorta (AO), gallbladder (GB), left/right adrenal glands (LA,RA), liver (LV), left/right kidney (LK,RK), pancreas (PN), spleen (SP), and stomach (ST). For validation, segmentation ground-truth is generated for 9 NA and 9 MO cases with ITK-Snap tool. Fig.1(b,c) illustrate the examples of the segmentation ground-truth. The probabilistic atlas is built with ten ( $K = 10$ ) abdominal thin-slice CT scans of normal anatomy delineated by expert radiologists.

### 3.2 Results

We first evaluate OLMs and OSMs that are built by using our data. To estimate each organ center, we use 3D center of gravity of  $B_l$  computed by our base MOS. Fig.2(a) shows an example view of the constructed NA in Eq(1). Fig.2(b)

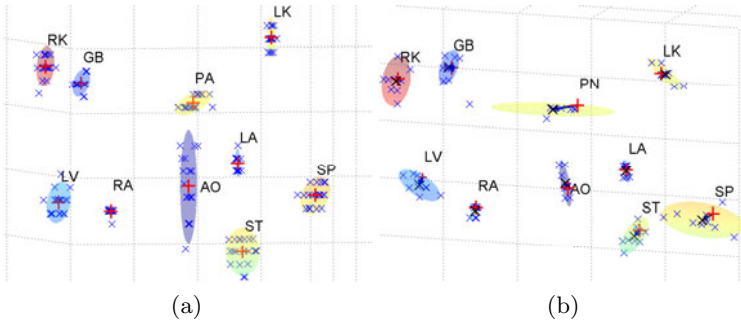


**Fig. 2.** OLM and OSM. (a) *NA* with 10 organs. Estimated organ and model centers are denoted by blue 'x' and red '+', respectively. An ellipse shows an iso-contour of the 3D covariance multiplied by two for each organ. (b) Detectional *OS* with the organ shift vectors shown in indigo arrows. *MO*'s and *NA*'s centers are denoted by black 'x' and red '+', respectively.

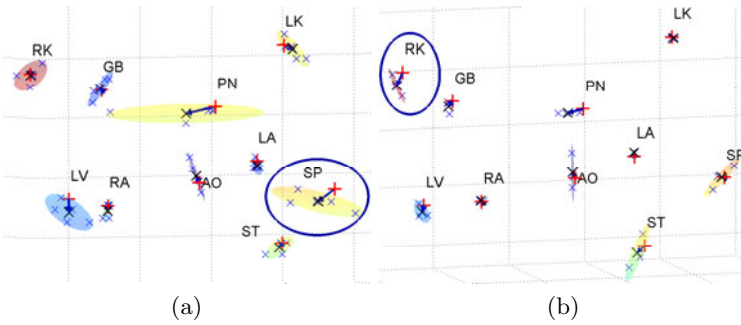


**Fig. 3.** Detectional  $OS_t$  for splenectomy and nephrectomy. (a) With five splenectomy cases. (b) With three nephrectomy cases. Blue ellipses show removed organs for respective procedures.

illustrates a similar example view of the detectional  $OS$  in Eq.(3). Next the surgical procedure-specific detectional OSMs are evaluated. Fig.3(a,b) show detectional  $OS_t$  for splenectomy and nephrectomy in the same format of Fig.2. Larger shifts are observed by the removed organs indicated by ellipses.

Quantitative analyses of constructed OLMs and detectional OSMs are evaluated in Fig.4. Fig.4(a) summarizes the variance of OLMs for each organ. The trace of a covariance matrix is equivalent to the sum of eigenvalues thus proportional to the average variance across the three spatial axes. For *NA*, the covariance trace for the stomach was the largest (92.8) and that for the left kidney was the smallest (4.2). For *MO*, the trace for the pancreas was the largest (428.7) and that for the left adrenal was the smallest (6.1). The unit of the measures is in voxels. The pancreas exhibited the largest magnitude of the organ shift (16.3), followed by the spleen (8.0), stomach (3.6), and aorta (3.2). Fig.4(b) compares the magnitudes of organ shift vectors  $y_{lm}$  for each organ. Pancreas and

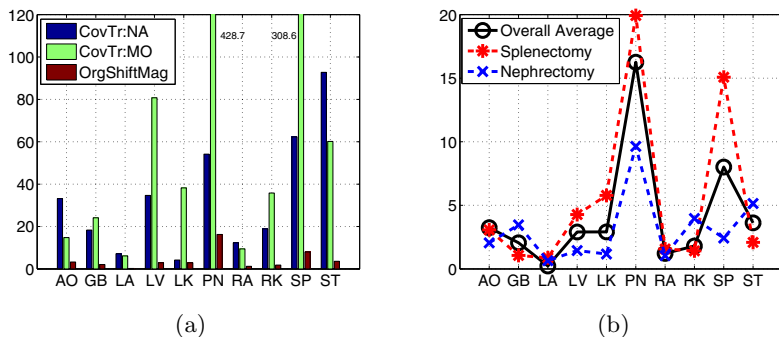


**Fig. 4.** Analyses of organ location variances and organ shift magnitudes. (a) Blue: trace of covariances in *NA*, green: trace of covariances in *MO*, magenta: magnitudes of organ shift vectors in voxels. (b) Comparison of magnitudes of organ shift vectors in voxels for the two surgical procedures against the overall average.

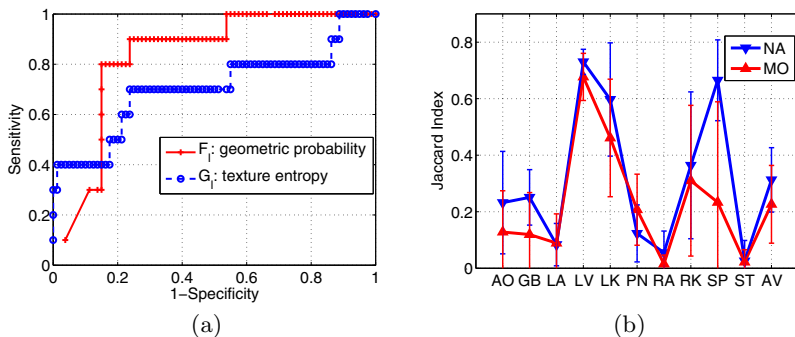


**Fig. 5.** (a) ROC analysis for missing organ detection with  $F_l$  and  $G_l$  features. (b) Segmentation accuracy in Jaccard index ( $JI$ ). Blue down-triangles and red up-triangles show organ-wise average  $JIs$  for *NA* and *MO* cases, respectively. Captions of organs are defined in Sec.3.1. 'AV' indicates the average  $JI$  over all organs.

spleen resulted in large organ shifts for both procedures. For splenectomy, pancreas, left kidney, liver and spleen exhibited the shifts larger than average. For nephrectomy, gall bladder, stomach and right kidney exhibited larger shifts. In both cases, organs that were removed (spleen and right kidney) resulted in large shifts, which indicate mismatch to non-target organ(s). Fig. 5(a) summarizes the receiver operating characteristic (ROC) analysis of missing organ detection using  $F_l$  in Eq.(4) and  $G_l$  in Eq.(5). Both features exhibit positive correlations to the missing organ occurrences. At 3.75% false positive rate (FPR), sensitivity for  $F_l$  and  $G_l$  are 10% and 40%. At 15% FPR, sensitivity for  $F_l$  and  $G_l$  are 80% and 40%. The area under the curve (AUC) for  $F_l$  and  $G_l$  are 0.83 and 0.71, respectively.

Finally, we evaluate the baseline MOS results on our data from the diseased population. Fig. 5(b) shows organ-wise segmentation accuracy in Jaccard index ( $JI = \frac{|A \cap B|}{|A \cup B|}$  where  $A$  and  $B$  are equal-length binary patterns) averaged over

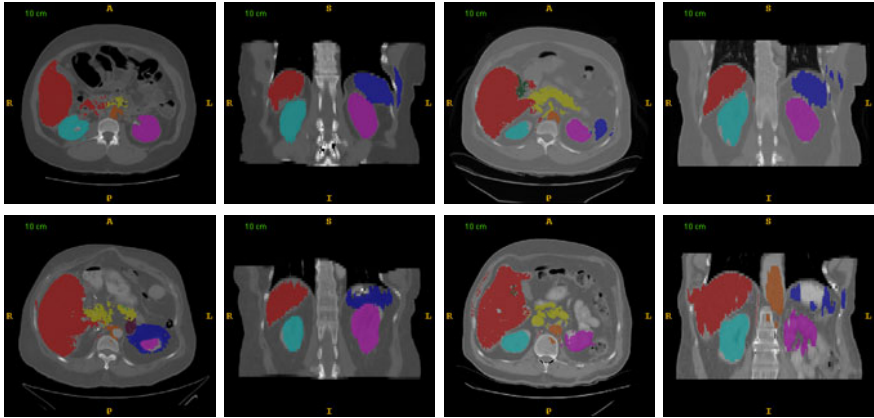


**Fig. 6.** Illustrative examples of the baseline atlas-guided MOS results. Top row: NA cases. Second row: spleen removed (left), spleen and left kidney removed (right). The same color scheme in Fig.1 is used.

the NA (blue 'V') and MO (red 'A') cases with ground truths. Liver, left kidney and spleen have relatively high accuracy. The accuracy for MO cases is lower than that for NA in general due to difficulties for handling the diseased cases. The accuracy for spleen and left kidney of MO is significantly lowered since MO includes cases missing them. Not only missing organ itself but even neighboring organ, liver, is influenced by right kidney missing such that the bottom of liver is segmented as right kidney that causes the lower accuracy of MO liver. Segmentation of adrenal glands and gall bladder is challenging because they are very small and their shape varies widely. Stomach also yields very low *JI* because its shape and intensity is extremely various.

Fig. 6 demonstrates four illustrative examples of segmentation results. NA cases shown in the top row indicate successful segmentations of major abdominal organs except for the pancreas in the left case. On the other hand, MO cases shown in the bottom row encountered more issues. On the splenectomy case on the left, the spleen model (blue) was falsely put on the left kidney and missed the aorta. On the splenectomy/nephrectomy case on the right, the spleen and left kidney models are falsely put on the stomach and intestine moved to the cavity vacated by the removed organs. In both cases, liver and right kidney are segmented correctly.

## 4 Conclusions and Discussion

This paper presented novel methods for modeling abdominal organ shifts due to surgical procedures and for detecting occurrence of missing organs. Our experimental results are promising in that 1) organ shift models depicted different patterns of organ movements for splenectomy and nephrectomy and 2) two features applied for detection exhibited reasonable accuracy with different patterns. Texture entropy performed better in low FPR while geometric probability performed better in higher FPR. Our future work includes building and analyzing

OLMs and OSMs with a larger dataset and exploring a combined feature with the two proposed as well as others. Finally, the resulting missing organ detection will be integrated with our overall MOS scheme in order to improve segmentation accuracy for the targeted diseased population.

## References

1. Dempster, A.P., Laird, N.M., Rubin, D.B.: Maximum likelihood from incomplete data via the EM algorithm. *J. Roy. Stats. Soc. Series B* 39, 1–38 (1977)
2. Guld, M.O., Kohnen, M., Keysers, D., Schubert, H., Wein, B.B., Bredno, J., Lehmann, T.M.: Quality of DICOM header information for image categorization. In: *SPIE*, vol. 4685, pp. 280–287 (2002)
3. Kobashi, M., Shapiro, L.G.: Knowledge-based organ identification from CT images. *Pattern Recognition* 28, 475–491 (1995)
4. Kobatake, H.: Future CAD in multi-dimensional medical images - project on multi-organ, multi-disease CAD system. *Computerized Medical Imaging and Graphics* 31, 258–266 (2007)
5. Lee, C.C., Chung, P.C., Tsai, H.M.: Identifying multiple abdominal organs from CT image series using a multimodule contextual neural network and spatial fuzzy rules. *IEEE Trans. Info. Tech. in Biomed.* 7, 208–217 (2003)
6. Linguraru, M.G., Pura, J.A., Chowdhury, A.S., Summers, R.M.: Multi-Organ Segmentation from Multi-Phase Abdominal CT via 4D Graphs using Enhancement, Shape and Location Optimization. In: Jiang, T., Navab, N., Pluim, J.P.W., Viergever, M.A. (eds.) *MICCAI 2010, Part III. LNCS*, vol. 6363, pp. 89–96. Springer, Heidelberg (2010)
7. Linguraru, M.G., Sandberg, J.K., Li, Z., Pura, J.A., Summers, R.M.: Atlas-based automated segmentation of spleen and liver using adaptive enhancement estimation. *Medical Physics* 37, 771–783 (2010)
8. Liu, X., Linguraru, M.G., Yao, J., Summers, R.M.: Organ pose distribution model and an MAP framework for automated abdominal multi-organ localization. In: *Proc. Medical Imaging and Augmented Reality*, pp. 393–402 (2011)
9. Okada, T., Yokota, K., Hori, M., Nakamoto, M., Nakamura, H., Sato, Y.: Construction of Hierarchical Multi-Organ Statistical Atlases and their Application to Multi-Organ Segmentation from CT Images. In: Metaxas, D., Axel, L., Fichtinger, G., Székely, G. (eds.) *MICCAI 2008, Part I. LNCS*, vol. 5241, pp. 502–509. Springer, Heidelberg (2008)
10. Park, H., Bland, P.H., Meyer, C.R.: Construction of an abdominal probabilistic atlas and its application in segmentation. *IEEE Trans. Medical Imaging* 22, 483–492 (2003)
11. Rueckert, D., Sonoda, L.I., Hayes, C., Hill, D.L.G., Leach, M.O., Hawkes, D.J.: Non-rigid registration using free-form deformations: Application to breast MR images. *IEEE Trans. Medical Imaging* 18, 712–721 (1999)
12. Seifert, S., Barbu, A., Zhou, S.K., Liu, D., Feulner, J., Huber, M., Suehling, M., Cavallaro, A., Comaniciu, D.: Hierarchical parsing and semantic navigation of full body CT data. In: *Proc. SPIE Conf. Medical Imaging* (2008)
13. Shimizu, A., Ohno, R., Ikegami, T., Kobatake, H., Nawano, S., Smutek, D.: Segmentation of multiple organs in non-contrast 3D abdominal CT images. *Int. J. CARS* 2, 135–143 (2007)
14. Yao, J., Summers, R.M.: Statistical Location Model for Abdominal Organ Localization. In: Yang, G.-Z., Hawkes, D., Rueckert, D., Noble, A., Taylor, C. (eds.) *MICCAI 2009, Part II. LNCS*, vol. 5762, pp. 9–17. Springer, Heidelberg (2009)
15. Zhou, Y., Bai, J.: Multiple abdominal organ segmentation: An atlas-based fuzzy connectedness approach. *IEEE Trans. Info. Tech. in Biomed.* 11, 348–352 (2007)